Materials Science-Poland, 41(1), 2023, pp. 27-41
http://www.materialsscience.pwr.wroc.pl/
DOI: 10.2478/msp-2023-0002

Structural, morphological, and optical properties of Ag_xO thin films deposited via obliquely angle deposition

H. Ben Soltane[1,2,*], F. Chaffar Akkari[1], B. Gallas[3], M. Kanzari[1,4]

[1]Université Tunis El Manar, Ecole Nationale d'Ingénieurs de Tunis, Laboratoire de Photovoltaïque et Matériaux Semiconducteurs, BP37, 1002 Le Belvédère, Tunis, Tunisia

[2]Ecole Nationale Supérieure d'Ingénieurs de Tunis, Université de Tunis, 5 Avenue Taha Hussein, 1008 Tunis, Tunisia

[3]Sorbonne Université, CNRS, Institut des Nanosciences de Paris – UMR 7588Campus Pierre et Marie Curie, Case 840, 04 place Jussieu 75005 Paris, France

[4]Université de Tunis, Institut Préparatoire aux Etudes d'Ingénieurs de Tunis-IPEIT, 2, Rue Jawaher Lel Nehru, 1089 Montfleury, Tunisia

This work reports on the optical, structural, and morphological properties of silver oxide thin films obtained by post-oxidation of silver deposited previously by the thermal evaporation technique. The samples were deposited on glass substrates using the oblique angle deposition technique for different angles of incidence γ (γ=0°, 20°, 40°, 60°, 75°, and 85°). γ is defined as the angle between the particle flux and the normal to the substrate. The resulting thin films were annealed in the free air at two temperatures (300°C and 400°C). X-ray diffraction (XRD), scanning electron microscopy (SEM), and UV-visible-NIR spectrophotometer were performed to study the crystal structure, as well as the morphological and optical properties (transmittance and reflectance), of the Ag_xO samples. X-ray diffraction analysis revealed the presence of the Ag_xO phase for the silver films deposited at a high angle of incidence and for the annealing temperature 300°C. In contrast, the diffractograms of the silver films annealed at 400°C show an amorphous behavior. Optical results indicated that the direct band gap energy increases pursuant to increasing the angle of incidence γ. The absorption coefficients of Ag_xO thin films were found to be in the range of 10^3–10^5 cm^{-1}. Additionally, we determined the birefringence for the layers annealed at 400°C and found that the highest value of birefringence is obtained corresponding to the angle of incidence 60°. Morphological analysis indicated that the porosity increases with the angle of incidence and highlights the amorphous nature of the films, which is attributed to the columnar structure.

Keywords: *obliquely angle deposition, silver oxide, nanocolumnar Ag_xO thin films, structural characterization, optical analysis, morphological properties*

1. Introduction

The study of silver oxides, in particular in their thin film form, presents a great deal of interest to researches owing to their unique properties and new applications in gas sensors [1], optical storage devices [2], photovoltaic cells [3], photodiodes [4], etc. [5]. Additionally, they are also used as substrates for Raman scattering (SERS) in plasmonic devices [6]. It has been found that silver has different oxidation states and forms multiple oxides: AgO, Ag_2O, Ag_3O_4, and Ag_2O_3, which represent a fascinating group of inorganic materials [7]. It is particularly important to know that the most stable phase is Ag_2O [8]. The crystalline structures of these oxides exhibit different geometries, and it is possible to harness this phenomenon in a way that enables achieving distinct architectural, electrical, or optical features [9]. Silver oxide is transparent in the infrared and in the visible as a result of its high optical band gap [10]. This characteristic makes it suitable for achieving better performance compared to other metallic films in optical applications. Many methods are applied to deposit silver oxide thin films, especially thermal evaporation [11], chemical vapor deposition (CVD) [12], reactive magnetron sputtering (RMS) [13], and pulsed laser deposition [14] techniques. Physical vapordeposition (PVD) is generally performed by thermal

* E-mail: bensoltanehejer@gmail.com

© Ben Soltane et al. 2023. This is an open access article distributed under the Creative Commons Attribution-NonCommercial-NoDerivatives 4.0 License. (http://creativecommons.org/licenses/by-nc-nd/4.0/)

evaporation under vacuum. This process involves the deposition of thin films in a vacuum to apply pure material layers to the surface of various substrates. Some of the major advantages of thermal evaporation are its high deposition rates, simple operation, and relatively low equipment cost. Glancing angle deposition (GLAD) represents an innovative and interesting technique for the production of nanostructured materials at a low cost based on deposition under oblique incidence (OAD) [15]. The general principle is based on the spatial orientation of the substrate while the source remains fixed. The center of the substrate is generally aligned with the vapor source, which allows easy control of the orientation. The oblique deposition angle γ is defined as the angle of deposition between the incident flux and the vertical to the substrate. From this technique, it is possible to develop new nanostructures with different architectural arrangements such as inclined columns [16], zigzag shapes [17], helixes [18], and nano spirals [19]. Effectively, the GLAD offers many opportunities for the control of the structure and porosities,as well as for increasing the anisotropy of the resulting thin films, which enables the development of new applications [5, 20]. Anti-reflection layers, Bragg effect reflectors, nanophotonic products, and nanoscale sensors [21] may be mentioned as a few examples of applications requiring thin films characterized by such a porosity and nanostructure. With this technique, the control of the angle of incidence enables the creation of anisotropic optical characteristics. In a recent work, it has been proven that it is possible for a variety of different materials deposited at oblique angles of incidence to exhibit characteristics such as bichromaticity, birefringence, and anisotropic properties that may be useful in several applications. Thanks to this method, the orientation of the column, the porosity of the treated thin films, and then the physicochemical properties of the layers can be precisely adjusted, thus allowing new interesting applications, such as photovoltaic solar cells [22], gas sensors [23], photonic crystals [24], photo catalysis [25], and optical filters [26]. The objective of this work is to realize nano thin films sculpted of silver by the GLAD technique, obtained by thermal evaporation under vacuum in oblique incidence on glass substrates inclined at a variable angle of incidence, followed by an annealing process at different temperatures in free air without rotating the substrate. The structure, the composition, and the crystallinity of the films will be determined by X-ray diffraction (XRD) andscanning electron microscopy (SEM). The optical properties of these thin films will be studied based on spectrophotometer measurements. In this article, we have attempted all of the analysis results used to investigate the effect of oblique angle deposition and annealing temperature on Ag_xO films.

2. Experimental details

2.1. Ag_xO thin film preparation

Evaporation of silver was carried out on rectangular shaped glass substrates (2.5×1.5 cm^2). The glass substrates are cleaned first with commercial detergent, then with acetone, and finally with dilute hydrochloric acid solution; thereafter they are rinsed with ethanol, and finally with demineralized water. The thin layers of Ag were deposited by the technique of thermal evaporation under vacuum under a pressure of 10^{-6} Torr, at an oblique angle for multiple specific angles of incidence (γ=0°, 20°, 40°, 60°, 75°, and 85°). Thus, and to ensure uniform deposition on the substrate, the distance between the source of evaporation and the substrate has been set at approximately 11 cm. A simplified diagram of the GLAD technique and nanocolumns is shown in Figure 1. All the silver films thus formed were introduced into a programmable oven and annealed in the free air at 300°C and 400°C for 3 hr to form silver oxide films.

2.2. Characterization techniques of the Ag_xO thin films

The different characterizations, including the structural, optical, and morphological properties of thin films, have been investigated using different techniques. The prepared Ag_xO layers were studied by the XRD technique using a Philips X'Pert X-ray diffractometer (40 kV, 30 mA, and CuKα radiation λ=0.154056 nm) in the range 2θ=10°–60°, in order to examine the crystalline structure of the ob-

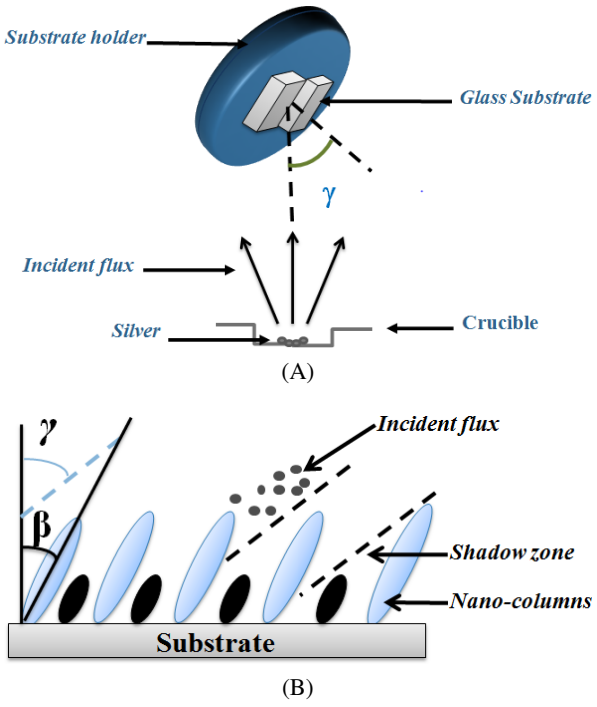


Fig. 1. **(A)** The schematic diagram of the GLAD technique, and **(B)** diagram of the self-shadowing effect during the growth of the layer. GLAD, glancing angle deposition

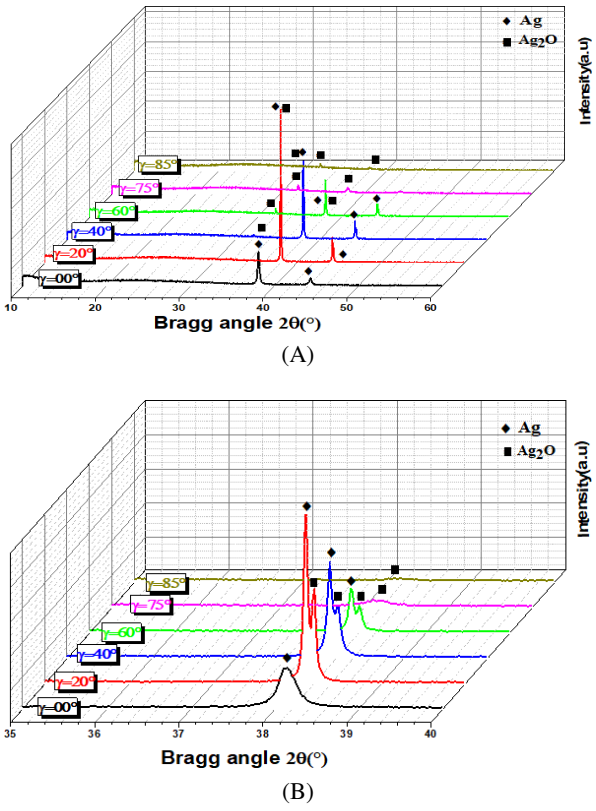


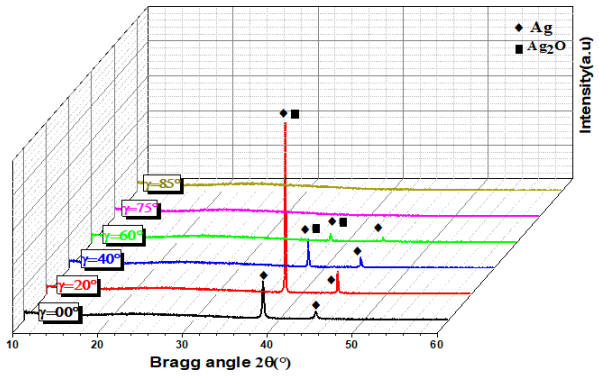
Fig. 2. **(A)** XRD patterns of Ag_xO thin films deposited, respectively, at γ=0°, 20°, 40°, 60°, 75°, and 85° annealed at 300°C, and **(B)** XRD patterns of Ag_xO thin films in the Bragg angles range 35°–40°. XRD, X-ray diffraction

tained samples. The surface morphology and cross-section structure of the samples were evaluated by SEM (ZEISS Supra 40), operating at an accelerating voltage of 5kV to control the nanostructures of the samples. Moreover, the samples were cleaved along the deposition plane and SEM was performed in the cross-section configuration to study the influence of the inclination of the substrate during deposition on the resulting microstructure. Measurements of the optical properties, transmittance, and reflectance of the obtained films were carried out using an UV-visible-NIR (Shimadzu 3100 S) spectrophotometer equipped with an integrated sphere in the wavelength spectral range 300–1,800 nm.

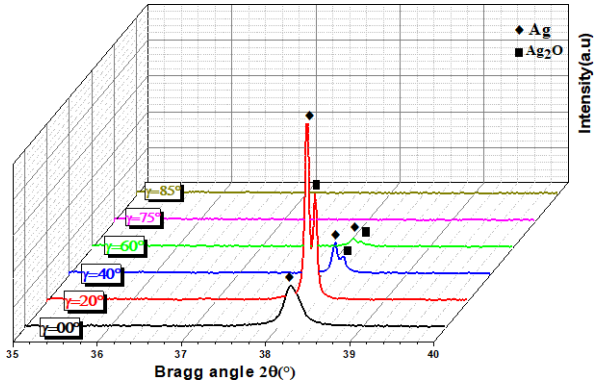
3. Results and discussion

3.1. Structural properties

XRD analysis was carried out on six samples corresponding to the annealing temperature 300°C (Figure 2) for different angles of incidence (γ=0°, 20°, 40°, 60°, 75°, and 85°) and annealed at 3 hr. XRD patterns of all the samples show crystalline nature. At low deposition angle γ=0°, only the silver phase can be observed with the presence of two peaks corresponding to (111) and (200) and identified to the cubic Ag phase with an intense peak at 2θ=38.1° according to the standard JCPDS card (01-001-1167). Additionally, and from Figure 2A, we can note that some of the lines are set very close together (Figure 2B). We can notice that the major peak is composed of two associated peaks, indicating the persistence of the metallic silver phase, Ag, accompanied by the appearance of silver dioxide, Ag_2O [27], corresponding to the Bragg angle 2θ=38.2°assigned to JCPDS card 01-075-1532. It is seen also that as the deposition angle increases (γ=40°, 60°, 75°, and 85°), Ag_2O becomes the dominating oxide, with the presence



(A)



(B)

Fig. 3. **(A)** XRD patterns of Ag_xO thin films deposited, respectively, at γ=0°, 20°, 40°, 60°, 75°, and 85° annealed at 400°C, and **(B)** XRD patterns of Ag_xO thin films in the Bragg angles range 35°–40°. XRD, X-ray diffraction

Table 1. Different phases, Bragg angles, and reticular planes (hkl) of the samples for the incident angles γ=0°, 20°, 40°, 60°, 75°, and 85° and the incident angles γ=0°, 20°, 40°, and 60° for the annealing temperatures 300°C and 400°C, respectively

Annealing temperature (°C)	Deposition angle γ (°)	Bragg angle 2θ(°)	Phases	(hkl)
300	00	38.1	Ag	(111)
	20	44.3	Ag	(200)
	40	38.1	Ag	(111)
	60	38.2	Ag_2O	(200)
	75	44.3	Ag	(200)
	85	32.2	Ag_2O	(111)
		38.1	Ag	(111)
		38.2	Ag_2O	(200)
		44.3	Ag	(200)
		32.2	Ag_2O	(111)
		38.1	Ag	(111)
		38.2	Ag_2O	(200)
		44.3	Ag	(200)
		32.2	Ag_2O	(111)
		38.2	Ag_2O	(200)
		44.4	Ag	(200)
		32.2	Ag_2O	(111)
		38.2	Ag_2O	(200)
400	00	38.1	Ag	(111)
	20	44.4	Ag	(200)
	40	38.1	Ag	(111)
	60	38.2	Ag_2O	(200)
		44.3	Ag	(200)
		38.1	Ag	(111)
		38.2	Ag_2O	(200)
		44.3	Ag	(200)
		38.1	Ag	(111)
		38.2	Ag_2O	(200)
		44.3	Ag	(200)

of another peak that becomes more and more intense located at the angular position 2θ=32.2°. For the high incidence angles γ=75° and 85°, we can notice that we have approximatively a disappearance of the metallic phase Ag. Therefore, we can conclude that for these high incidence angles, the formation of the silver oxide is favorized. In Table1, we present the different phases, the Bragg angles, and the reticular planes (hkl) for the different deposition angles. On the other hand, XRD analysis was performed on six layers annealed at 400°C for 3 hr for the same incidence angles. The X-ray patterns are shown in the Figure 3. For these layers (Figures 3A and 3B), it can be noticed that the increase of the annealing temperature modifies the structure and leads to the formation of the silver oxide only for the incidence angles γ=20°, 40°, and 60°. For the incidence angles γ=75° and 85°, the patterns do not show any peaks of the Ag_xO and the samples are amorphous.

Moreover, for the three angles γ=20°, 40°, and 60°, we have the same patterns, where there is a disappearance of the peak 2θ=32.2°. Thus, it can be noticed that the Ag_xO films deposited at low incident angles are relatively crystallized, in contrast to the films deposited at high incident angles, which are amorphous. This character can be explained by the nanocolumn structures produced by GLAD technique which leads to the increase in the number of defects due to the void between inclined

Table 2. Structural data of nanocolumnar silver oxide thin films for the incident angles γ=0°, 20°, 40°, 60°, 75°, and 85°, and with the annealing temperature at 300°C and 400°C

Annealing temperature (°C)	**Deposition angle γ (°)**	**Crystallite size (nm)**	**Strain $\varepsilon(\times 10^{-3})$**	**Dislocation density $(\delta)(\times 10^{-3})$ (nm^{-2})**
	00	36	2.95	0.77
	20	55	1.92	0.33
	40	51	2.09	0.38
300	60	54	1.95	0.34
	75	26	3.97	1.47
	85	27	3.90	1.37
400	00	37	2.81	0.73
	20	57	1.96	0.30
	40	51	2.09	0.38
	60	55	1.97	0.32
	75	–	–	–
	85	–	–	–

nanocolumns [28]. Annealing at 300°C shows that more the angle increases more the Ag phase decreases and silver oxide becomes dominant. Therefore, this technique has favored the formation of Ag_2O.

As a result, silver oxidation could be enhanced by deposition at higher oblique incidence angles. This could be attributed to the larger surface area in contact with free air than that obtained by deposition at normal incidence. In the samples deposited at low incidence, the presence of the metallic phase of silver indicates partial oxidation. The same findings were also validated in the copper oxide thin films deposited using the GLAD technique [29].

In order to further investigate the structural properties of the developed samples at 300°C and 400°C, we have calculated some parameters such as crystallite size, strain, and dislocation density. All these values are presented in Table 2.

The crystallite size of the films was calculated using the Debye–Scherrer formula [30]:

$$D = \frac{0.9\lambda}{\beta \cos\theta}$$

The crystallite size has been determined using a Gaussian function to fit the peaks in the XRD patterns, where λ is the X-ray wavelength, θ is the Bragg diffraction angle, and is β the full-width at half-maximum (FWHM) of the peak corresponding to θ.

The strain of the layers was determined using the following formula [31]:

$$\varepsilon = \frac{\beta}{4\tan\theta}$$

The dislocation density of the obtained samples has been estimated using the following formula [32]:

$$\delta = \frac{1}{D^2}$$

Thin films annealed at 400°C show amorphous behavior for the two strong angles 75° and 85° (see Figure 3 and Table 2). At other angles, 0°, 20°, 40°,

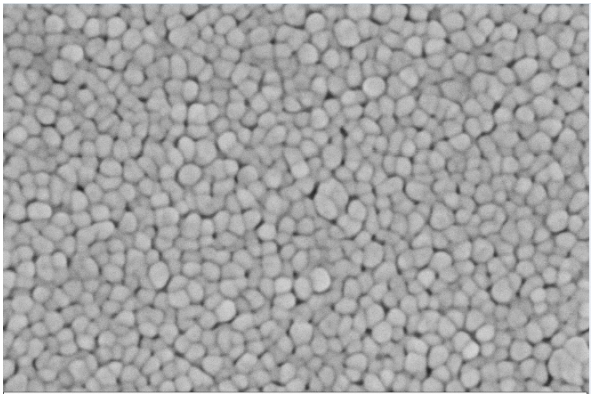


Fig. 4. Surface morphology of silver thin film before annealing for the incident angle γ=0°

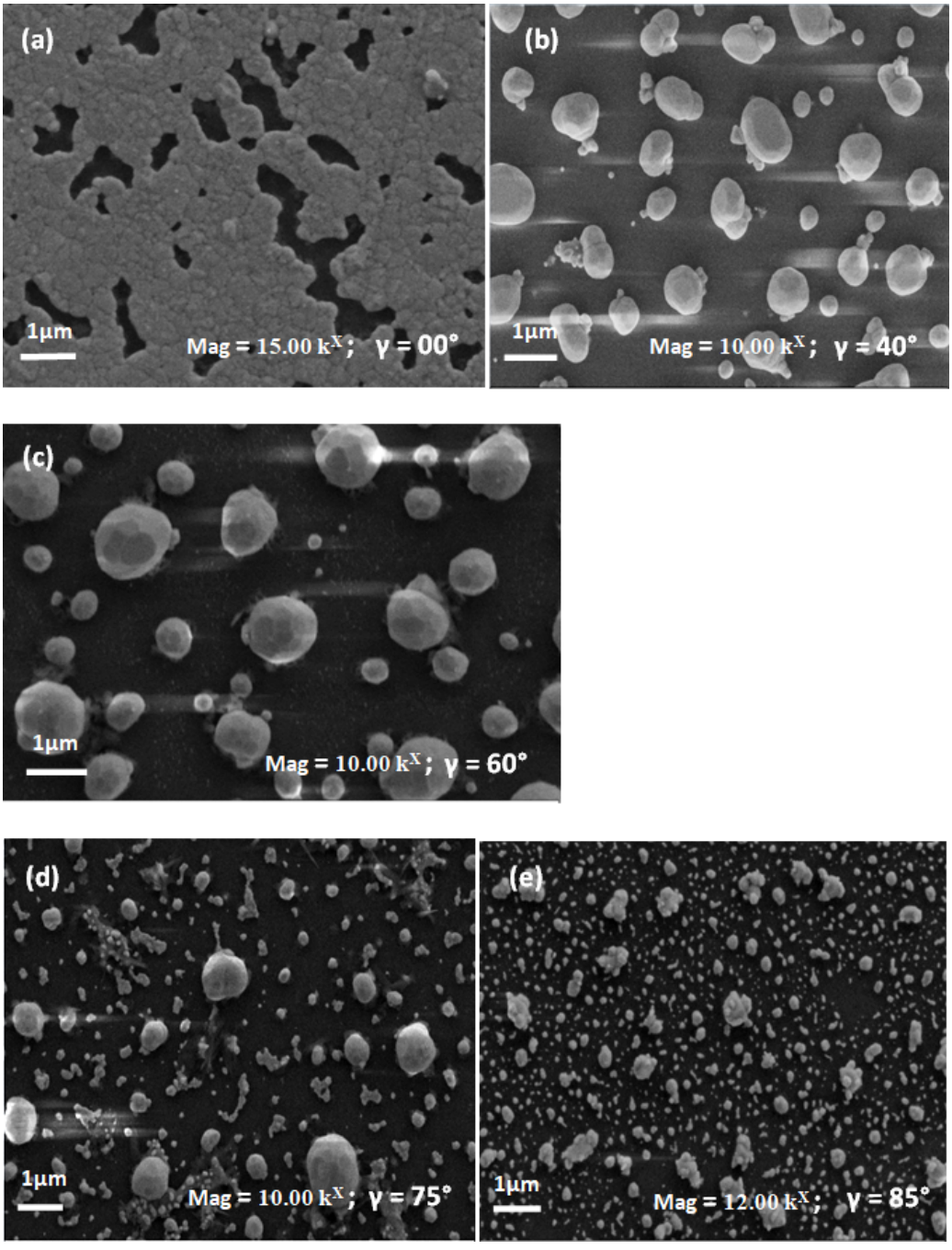


Fig. 5. Surface morphologies of silver oxide thin films after annealing at 300°C for the incident angles a=(γ=0°), b= (γ=40°), c=(γ=60°), d=(γ=75°), and e=(γ=85°)

and 60°, it was possible to detect the presence of diffraction peaks indicating a polycrystalline structure, and so the crystallite size was calculated. The values are between 37 nm and 57 nm. The annealed thin films at 300°C are all polycrystalline; the crystallite size values could be determined for all angles (0°, 20°, 40°, 60°, 75°,and 85°), and they range from 27 nm to 55 nm (Table 2).

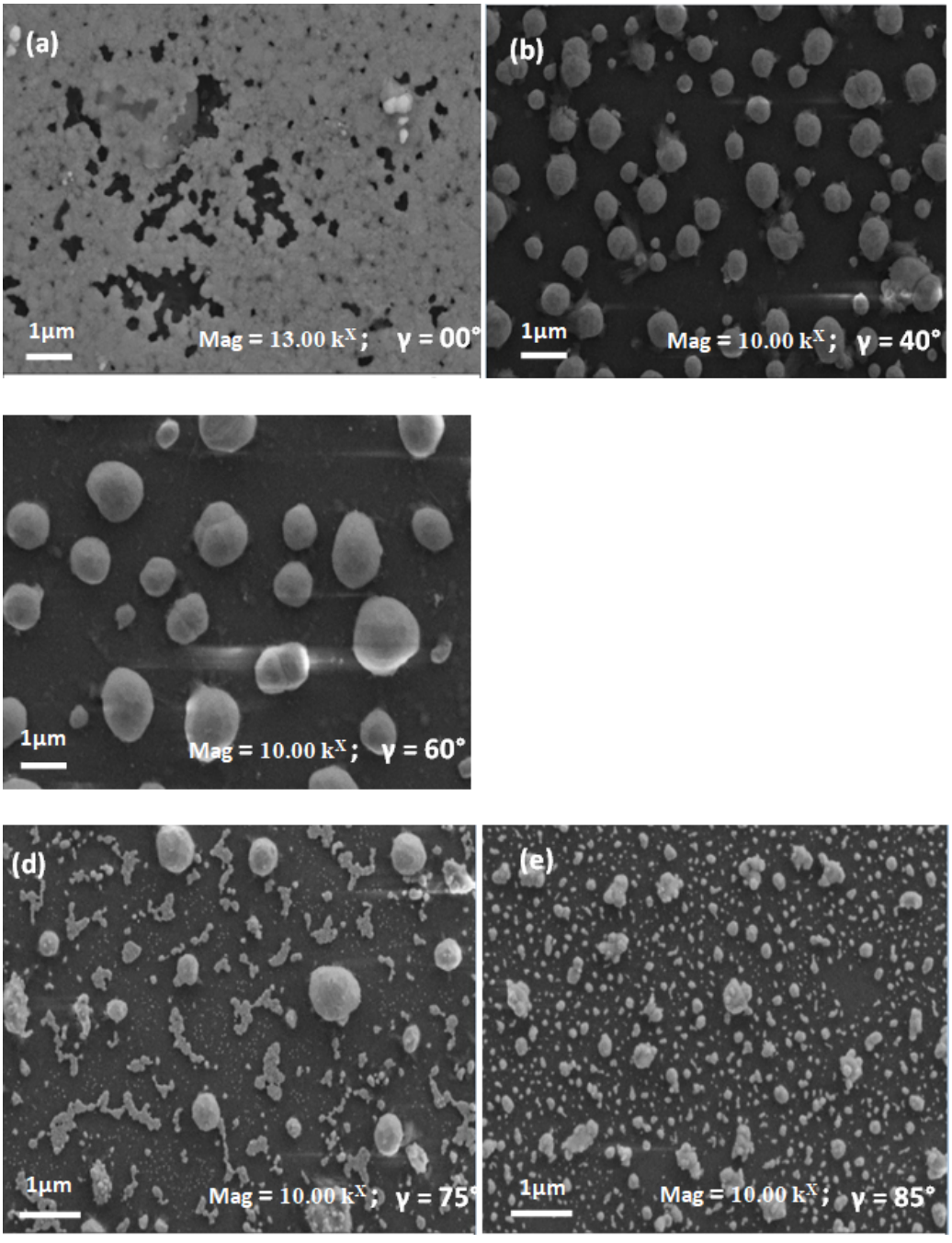


Fig. 6. Surface morphologies of silver oxide thin films after annealing at 400°C for the incident angles a=(γ=0°), b= (γ=40°), c=(γ=60°), d=(γ=75°), and e=(γ=85°)

3.2. Morphological properties

The SEM analysis technique has been performed to study the morphological properties of the prepared Ag_xO thin films on glass substrates. Figure 4 shows how the silver is distributed before thermal annealing under free air, showing a homogeneous smooth surface consisting of densely packed grains. Figures 5 and 6 show micrographs of Ag_xO thin films prepared after thermal annealing under free air for the samples deposited at γ=0°,

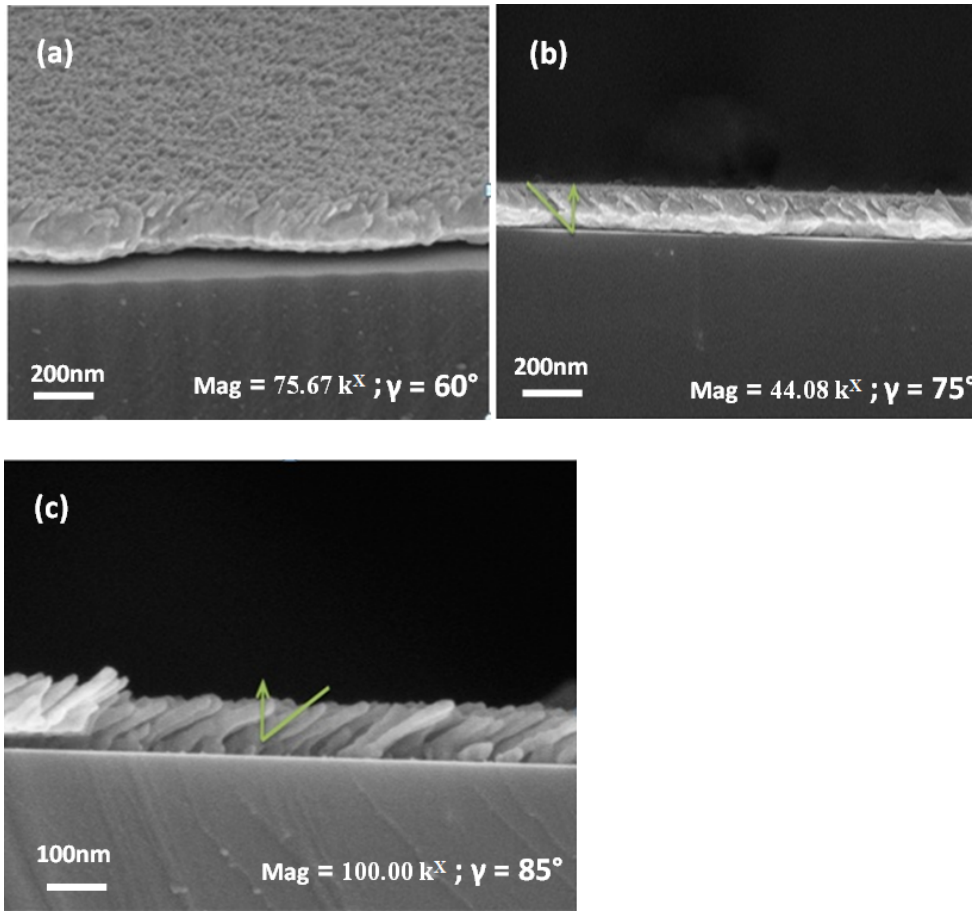


Fig. 7. Cross-section of Ag_xO thin films deposited at incident angles**(A)**γ= 60°, **(B)**γ=75°, and **(C)**γ=85°

40°, 60°, 75°, and 85°, respectively, at 300°C and 400°C. The surface morphology showed a dominance of the metallic phase (Ag) at the incident angle γ=0°. By increasing the incidence angle, the crystallite size becomes more defined and shows a mixture of small and big spherical granules. The size of the bigger grains seems to decrease as the deposition angle increases [7]. Examining the cross-section of the obtained films has permitted us to observe the films' nanostructure behavior. The cross-sectional SEM images of Ag_xO thin films prepared for the high incident angles γ=60°, 75°, and 85° are shown in Figure 7. Figures 7A–7C show that the films prepared by the oblique angle deposition technique are formed of columns inclined in the direction of the incident vapor separated by empty spaces. The same behavior has been reported in previous studies [33]; the inter-column spaces increase as the flow angle increases. This is the result of a shadowing effect, with a lot of pores. We can therefore conclude that the morphological characteristics are enhanced by the shadow effect and limited by the surface diffusion of the ad-atoms during the film development. Thus, this phenomenon generates porous films [34].

3.3. Optical properties

3.3.1. Transmittance and reflectance spectra

In order to investigate the effect of the incident deposition angle γ and the annealing temperature on the optical properties of the Ag_xO thin films, their optical parameters such as transmittance, reflectance, absorption and extinction coefficients, refractive index, optical band gap, and birefringence were studied. Figures 8 and 9 illustrate the transmittance T and reflectance R spec-

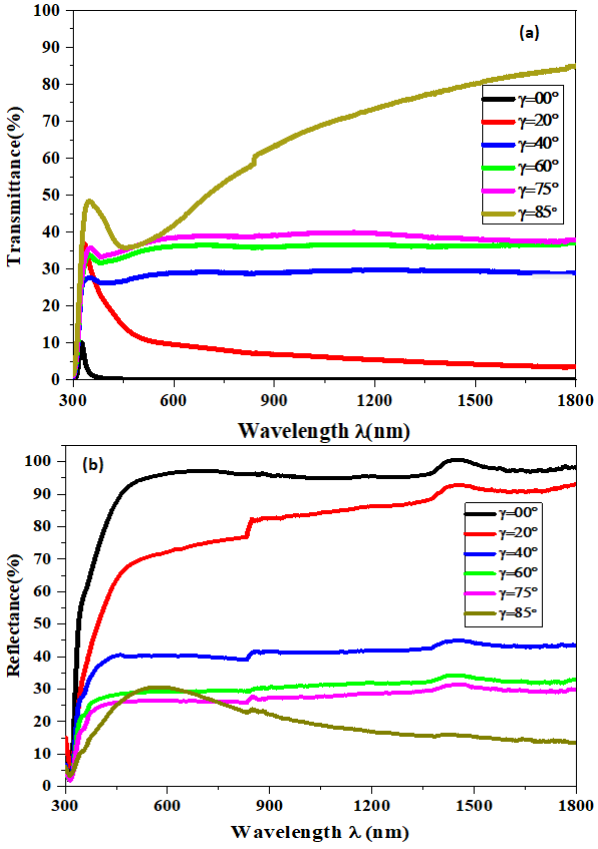


Fig. 8. **(A)** Transmittance spectra and **(B)** reflectance spectra of Ag_xO films deposited, respectively, at γ=0°, 20°, 40°, 60°, 75°, and 85° for the annealing temperature in free air of 300°C, for silver thin films

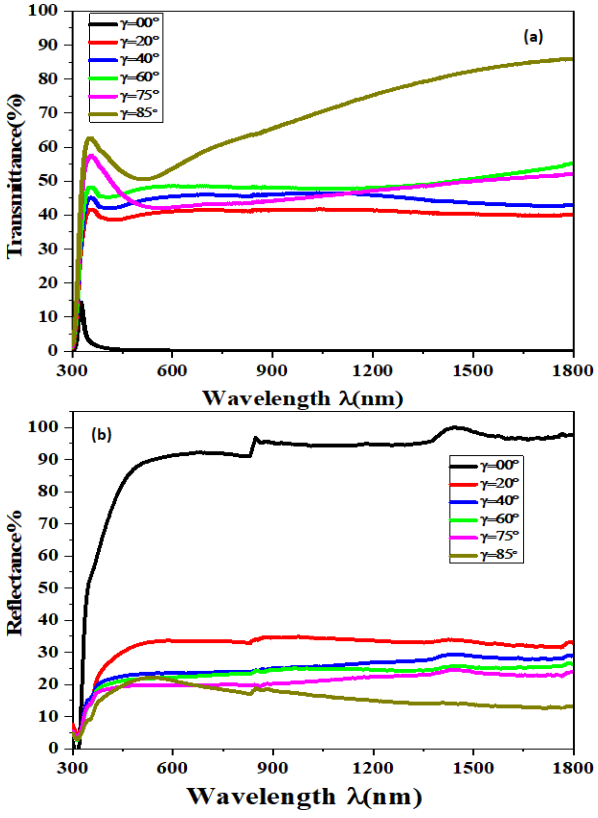


Fig. 9. **(A)** Transmittance spectra and **(B)** reflectance spectra of Ag_xO films deposited, respectively, at γ=0°, 20°, 40°, 60°, 75°, and 85° for the annealing temperature in free air of 400°C, for silver thin films

tra of Ag_xO thin films deposited at different incident angles (γ=0°, 20°, 40°, 60°, 75°, and 85°) and annealed at 300°C and 400°C under free air. The transmittance, T(λ), and reflectance, R(λ), of the deposited films were recorded in the wavelength spectral range 300–1,800 nm. It is clear from the Figures 8A and 9A that the T(λ) transmission spectra have the same form for the different angles of incidence. The two transmission spectra of the films deposited at γ=0° exhibit the lowest transmission values and we note that the transmittance increases as the incidence angle increases. For λ<700 nm, the transmittance values are in the range 10%–50%, which cover a part of the visible region, after which a large decrease in transmittance for wavelengths below 500 nm is observed due to the transition between the valence band and the conduction band. In the transparency region ($\lambda \geq$ 700 nm), the transmission reaches high values, of the order of 50%–85%, for the two annealing temperatures 300°C and 400°C. In comparison with other works [35, 36], the silver oxides were transparent in the visible range, with a maximum transmittance greater than 70%. We can therefore confirm the transparent character of the thin films, especially for the highest angles; and accordingly, confirmation for the presence of silver oxide is available. On the other hand, and from the reflection spectra (Figures 8B and 9B), an average reflection as a function of the angle of incidence was calculated in the range 400–1,800 nm. Please consider rephrasing for better clarity; the following is a provisional suggestion: “Based on Figure 10, we are able to infer that higher values of average reflection are manifest corresponding to lower in-

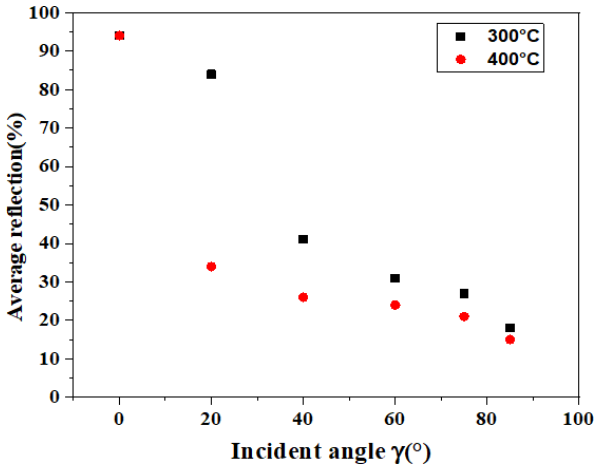


Fig. 10. Plot of average reflection for Ag_xO thin films deposited at different deposition angles (γ=0°, 20°, 40°, 60°, 75°, and 85°) annealed at 300°C and 400°C

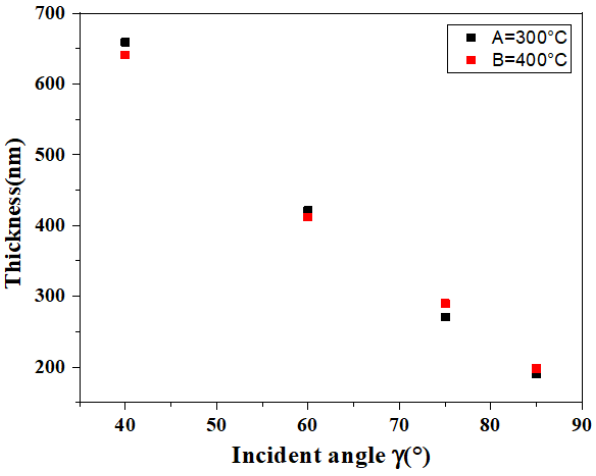


Fig. 11. The variation of the thickness for the incident angles γ= 40°, 60°, 75°, and 85° for the annealing temperatures **(A)** 300°C and **(B)** 400°C

cident angles, which can be explained by the presence of metallic silver, especially in the case of layers deposited at low incidence angles. For the high angles of incidence, the oxide phase dominates.

3.3.2. Thickness, extinction coefficient, refractive index, and birefringence

In the present study, the thickness, extinction coefficient, refractive index, and birefringence of Ag_xO thin films, deposited at incident angles γ=40°, 60°, 75°, and 85°, were calculated based on the transmittance and the reflectance spectra T(λ) by using the following equation [37]:

$$n_c = \left[n_s \times \left(\frac{1+\sqrt{R_{max}}}{1-\sqrt{R_{max}}} \right) \right]^{\frac{1}{2}}$$

where n_s is the refractive index of the glass substrate.

Thus, the thickness will be calculated based on the following rule [38]:

$$d = \frac{m\lambda}{4n_c}$$

Figure 11 illustrates the variation of the thickness versus the incidence angle (γ=40°, 60°, 75°, and 85°), and we can note that the thickness of the films decreases pursuant to an increase of the incident angle.

The extinction coefficient k can be calculated from the following relation [29]:

$$k = \frac{\alpha\lambda}{4\pi}$$

where α is the absorption coefficient and λ is the wavelength. The variation of extinction coefficient versuswavelength of the Ag_xO thin films deposited at different incident angles is shown in Figure 12. As can be seen, the extinction coefficient decreases pursuant to increase of the deposition angle. In the absence of oscillations, we can use this rule to calculate the refractive index [37]:

$$n = \frac{1+\left(1-\left(\frac{1-R}{1+R}\right)^2\left(1+k^2\right)\right)^{1/2}}{\frac{1-R}{1+R}}$$

Additionally, it can be noted that the refractive index of Ag_xO thin films decreases pursuant to increase of deposition angle. The decrease in refractive index and increase in transmittance are due to the porous structure of films deposited using the GLAD technique [39]. To highlight the presence of the silver metallic phase in the layers, we calculate $\delta n = n_{film} - n_{oxide}$ as the difference between the refractive index of the fabricated film and that of the silver oxide film free of the silver metallic phase. We took the value 2.1 for the refractive index of the oxide layer [7]. It is clear from Figure 13 that this deviation is large for low angles of

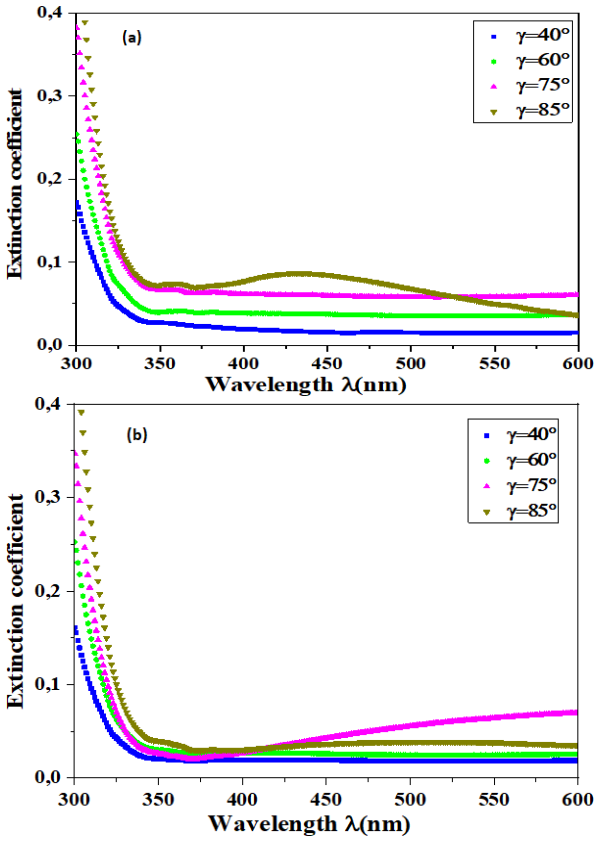


Fig. 12. Extinction coefficient spectra of films deposited at incident angles γ=40°, 60°, 75°, and 85° annealed in free air at **(A)** 300°C and **(B)** 400°C

incidence, which confirms the effect of the presence of the metallic phase silver. We clearly see that the annealing at 300°C does not entirely eliminate the metallic phase because δn is always positive (Figure 14). On the other hand, annealing at 400°C completely eliminates the metallic phase for high angles of incidence because δn is negative. Therefore,the more δn increases, the more the layers show a metallic-like feature. The birefringence was measured by studying the transmission spectra with two orthogonal directions of linearly polarized incident light; Tx is in the x-direction and Ty is in the y-direction for the thin films [40]. Indeed, in-plane birefringence is defined as the difference between the two in-plane refractive indices [40]. Figure 15 shows the variation of the plane birefringence $\Delta n = n_x - n_y$ for Ag_xO thin films deposited at different deposition angles (γ=0°, 20°, 40°, 60°, 75°, and 85°). Here, n_x and n_y are determined using the Swanepoel method [38]. As we can see, the birefringence is weak at a low incident angle, after which it increases by increasing the deposition angle and reaches a maximum value of Δn=0.259 at an angle γ=60°. In general, the maximum is obtained for the deposition angle of γ=60° [33], which appears as a critical angle. This maximum can be associated with the geometry of the columns. Consequently, the high deposition angle results in a more porous structure and this tends to decrease the value of birefringence [40]. It is interesting to note that,for the cases of GLAD-deposited ZrO_2 [41], WO_3 [42], and TiO_2 [40], the same behaviorwas observed. To conclude, the obliquely angled deposition method may present an excellent technique for producing films with controlled birefringence. Thus, it can be deduced that the anisotropic properties of the films deposited using this technique are linked to the biaxial columnar structures, as reported by Charles et al. [42].

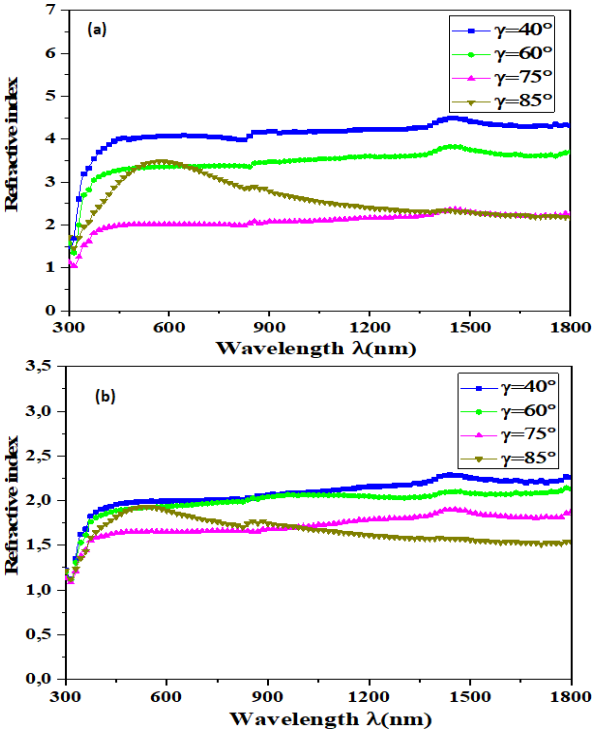


Fig. 13. Refractive index spectra of films deposited at incident angles γ=40°, 60°, 75°, and 85° annealed in free air at **(A)** 300°C and **(B)** 400°C

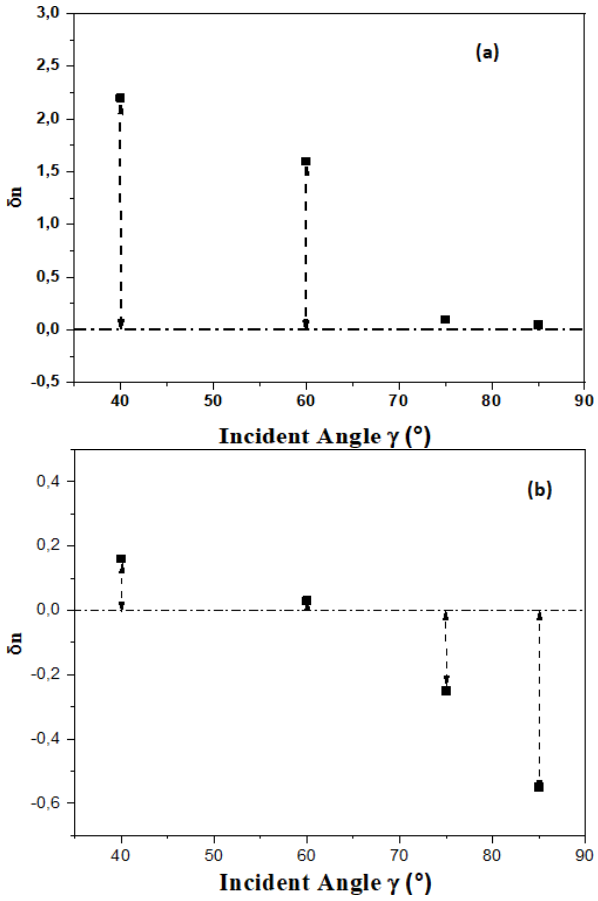


Fig. 14. Δn spectra of films deposited at incident angles γ=40°, 60°, 75°, and 85° annealed in free air at **(A)** 300°C and **(B)** 400°C

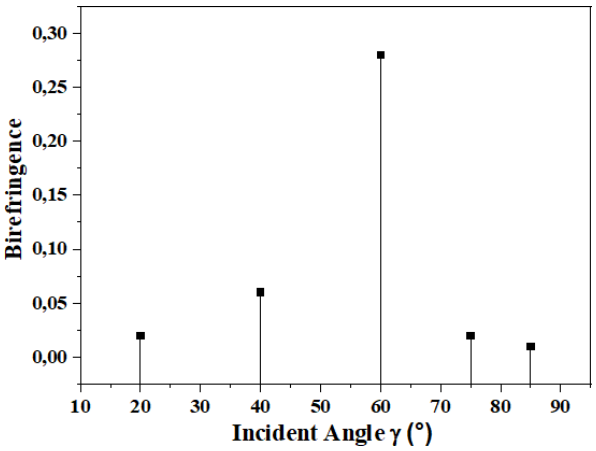


Fig. 15. The variation of the plane birefringence Δ*n* for Ag_xO thin films deposited at different deposition angles (γ=0°, 20°, 40°, 60°, 75°, and 85°) for the annealing temperature in free air 300°C, for silver thin films

3.3.3. Absorption coefficient and optical band gap

The absorption coefficient is one of the most important parameters in the consideration of silver oxide as an absorber material in the photovoltaic. The optical absorption coefficient αof Ag_xO nanocolumn thin films was calculated from the transmittance T(λ) and reflectance R(λ) data using the following relation [29]:

$$\alpha = \frac{1}{d} ln \left(\frac{(1-R)^2}{T} \right)$$

where *d* is the thickness of the layer.

Figure 16 shows the variation of the absorption coefficient (α) as a function of the photon energy for thin layers of silver oxide deposited on glass substrates at different incident angles prepared after thermal annealing under free air at 300°C (Figure 16A) and 400°C (Figure 16B). It is clear from this figure that the obtained silver oxide thin films have a relatively high absorption coefficient between 10^3 cm^{-1} and 10^5 cm^{-1} in the visible and near infrared spectral ranges. This result is very important to justify the transparency of the films. On the other hand, the absorption coefficient α can be related to the band gap energy *E*g according to the Tauc model [43]:

$$\alpha h\nu = A(h\nu - Eg)^q$$

where A is a constant that depends on the transition probability, α is the absorption coefficient, *hν* is the incident photon energy, *Eg* is the band gap energy, and *q* is a number that characterizes the transition processand is equal to 1/2 for permitted direct transitions and 2 for permitted indirect transitions. Figure 17 represents the variation of $(\alpha h\nu)^2$as a function of the photon energy *hν*. The extrapolation of the linear part of this curve with the abscissa axis permits us to estimate the difference values for the different layers obtained. The direct band gaps are almost stable values for the layers annealed at 300°C and 400°C for the anglesγ=40°, 60°, 75°, and 85°. The different val-

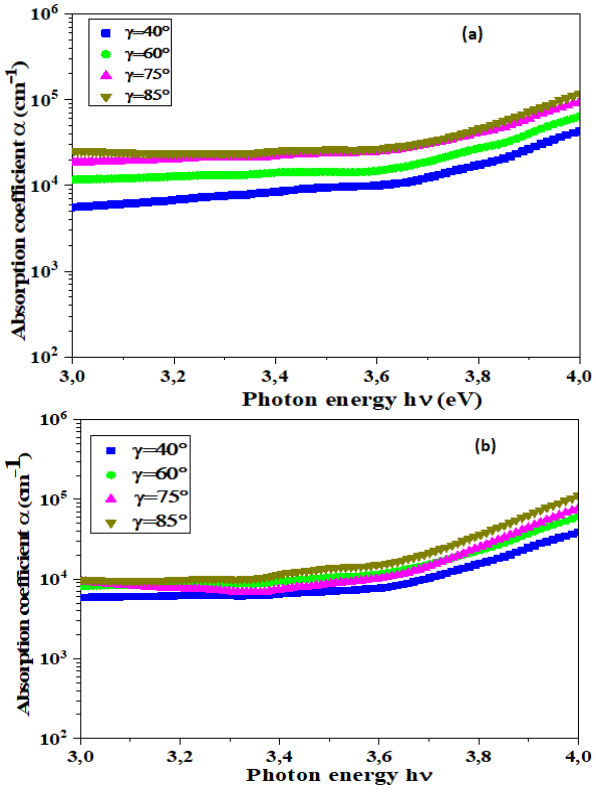


Fig. 16. Absorption coefficient spectra of films deposited at incident angles γ=40°, 60°, 75°, and 85° annealed in free air at **(A)** 300°C and **(B)** 400°C

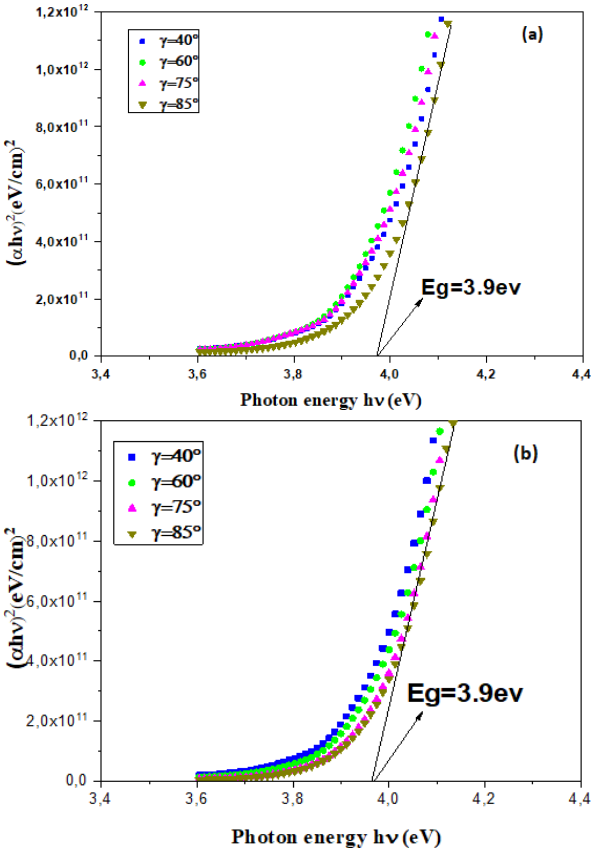


Fig. 17. Direct band gap energy spectra of films deposited at incident angles γ=40°, 60°, 75°, and 85° annealed in free air at **(A)** 300°C and **(B)** 400°C

ues of band gap energy obtained for Ag_2O are a function of the method used, and vary accordingly, for instance in the following increasing order, ascertained based on an examination of the literature: 1.4–1.5 eV [44], 2.25 eV [45], and 2.98–3.36 eV [46]. We note that the band gap values of the samples elaborated using the GLADtechnique are higher than the ones deposited at the normal incident angle [47]. The increase of the band gap value is a property of the samples developed using the GLAD technique, and it is attributable to the increased disorder and porous character of the films [45].

4. Conclusion

In the present study, the GLAD technique was used to deposit silver thin films on glass substrates at different incident angles (which were denoted as γ), subsequent to which they were annealed in free air to form silver oxide Ag_xO. The effects of incident angle γ and annealing temperature on the physical properties of silver oxide Ag_xO thin films were studied. We observe that annealing at 300°C favored the formation of the Ag_2O phase with the best crystallinity. The surface morphologies and the cross-section views show the presence of organized nanocolumns. The structural and morphological characterizations confirmed the presence of nanopores within silver oxide thin films, in particular for those deposited at a high incident angle. High absorption coefficients, higher than 10^4 cm^{-1},were found for the silver oxides,in particular for the high incident angle 85°,which shows the effect of the inclination of the columns on the absorption phenomena. For all silver ox-

ides, a slight increase in the band gaps can be observed pursuant to increase of the incident angle. Additionally, the silver oxides deposited using obliquely angled deposition enables highly oriented nanostructures to be developed, providing a benefit in terms of the creation of anisotropic properties. Indeed, higher birefringence value was observed for layers corresponding to an incident angle of around 60°. The greatly significant advantage of this technique is the production of porous areas in the layers. In fact, it has been shown that these zones increase with the angle of inclination of the substrates. Consequently, the effective surfaces increase and therefore the reactivity with gas increases, which endows these nanostructured layers with the potential for effective and interesting applications in various fields.

References

[1] Dellasega D, Casari CS, Vario F, Conti C, Bottani CE, Bassi AL. Nanostructured Ag_4O_4 thin films produced by ion beam oxidation of silver. *Appl Surf Sci*. 2013;266: 161–169. doi:10.1016/j.apsusc.2012.11.121.

[2] Fuji H, Tominaga J, Men L, Nakano T, Katayama H, Atoda N. A near-field recording and readout technology using a metallic probe in an optical disk. *Jpn J Appl Phys*. 2000;39: 980–981.

[3] Tselepis E, Fortin E. Preparation and photovoltaic properties of anodically grown Ag_2O films. *J Mater Sci*. 1986;21: 985–988. doi:10.1007/BF01117383.

[4] Kiazadeh A, Gomes HL, Rosa da Costa AM, Moreira JA, de Leeuw DM, Meskers SCJ. Intrinsic and extrinsic resistive switching in a planar diode based on silver oxide nanoparticles. *Thin Solid Films*. 2012;522: 407–411. doi:10.1016/j.tsf.2012.08.041.

[5] Tominaga J. The application of silver oxide thin films to plasmon photonic devices. *J Phys: Condens Matter*. 2003;15: R1101–1122.

[6] Raju NRC, Kumar KJ. Photodissociation effects on pulsed laser deposited silver oxide thin films: surface-enhanced resonance Raman scattering. *J Raman Spectrosc*. 2011;42: 1505–1509. doi:10.1002/jrs.2895.

[7] Nwanya AC, Ugwuoke PE, Ezekoye BA, Osuji RU, Ezema FI. Structural and optical properties of chemical bath deposited silver oxide thin films: role of deposition time. *J Spectrosc (Hindawi)*. 2013: Article ID 450820. doi:10.1155/2013/450820.

[8] Xiaoyong G, Mengke Z, Zengyuan Z, Chao C, Jiaomin M, Jingxiao L. Effects of hydrogen annealing on the microstructure and optical properties of single-phased Ag_2O film deposited using direct-current reactive magnetron sputtering. *Thin Solid Films*. 2011;519: 6620–6623.

[9] Sullivan KT, Wu C, Piekiel NW, Gaskell K, Zachariah MR. Synthesis and reactivity of nano-Ag_2O as an oxidizer for energetic systems yielding antimicrobial products. *Combust Flame*. 2013;160(2): 438–446.

[10] Lund E, Galeckas A, Azarov A, Monakhov EV, Svensson BG. Photoluminescence of reactively sputtered Ag_2O films. *Thin Solid Films*. 2013;536: 156–159. doi:10.1016/j.tsf.2013.04.026.

[11] Muhsien MA, Hamdan HH. Preparation and characterization of p-Ag2O/n-Si heterojunction devices produced by rapid thermal oxidation. *Procedia Energy*. 2012;18: 300–311. doi:10.1016/j.egypro.2012.05.041.

[12] Yuan Z, Dryden NH, Vittal JJ, Puddephatt RJ. Chemical vapor deposition of silver. *Chem Mater*. 1995;7: 1696–1702. doi:10.1021/cm00057a019.

[13] Her YC, Lan YC, Hsu WC, Tsai SY. The characteristics of reactively sputtered AgO_x films prepared at different oxygen flow ratios and its effect on super-resolution near-field properties. *Jpn J Appl Phys*. 2004;43: 267–272.

[14] Deng R, Li J, Kang HK, Zhang HJ, Wong CC. Laser directed deposition of silver thin films. *Thin Solid Films*. 2011;519: 5183–5187. doi:10.1016/j.tsf.2011.01.108.

[15] Liang JS, Chen SH, Lin EY, Luo DF, Jiang SJ. Morphology evolution of glancing angle deposition Ag films on nanosphere-array substrates: Kinetic Monte Carlo simulation. *Comput Mater Sci*. 2013;79: 31. doi:10.1016/j.commatsci.2013.06.014

[16] Sinaoui A, Akkari FC, Kanzari M. Investigation of the effect of obliquely incident deposition on structural, morphological and optical properties of $CuInS_2$ thin films. *Res Rev Mater Sci Chem*. 2013;2: 1–17.

[17] Rahchamani SZ, Dizaji HR, Ehsani MH. Study of structural and optical properties of ZnS zigzag nanostructured thin films. *Appl Surf Sci.* 2015;356: 1096–104. doi:10.1016/j.apsusc.2015.08.224.

[18] Hawkeyea MM, Brett MJ. Glancing angle deposition: fabrication, properties, and applications of micro- and nanostructured thin films. *J Vac Sci Technol*. 2007;25: 1317–1335. doi:10.1116/1.2764082.

[19] Robbie K, Sit JC, Brett MJ. Advanced techniques for glancing angle deposition. *J Vac Sci Technol B: Nanotechnol Microelectron*. 1998;16: 1115–1122. doi:10.1116/1.590019.

[20] Lopes C, Pedrosa P, Martin N, Barradas NP, Alves E, Vaz F. Study of the electrical behavior of nanostructured Ti–Ag, thin films, prepared by glancing angle deposition. *Mater Lett*. 2015;157: 188–192.

[21] Grüner C, Liedtke S, Bauer J, Mayr SG, Rauschenbach B. Morphology of thin films formed by oblique physical vapor deposition. *ACS Appl Nano Mater*. 2018;1: 1370–1376.

[22] Siyanaki FH, Dizaji HR, Ehsani MH, Khorramabadi S. The effect of substrate rotation rate on physical properties of cadmium telluride films prepared by a glancing angle deposition method. *Thin Solid Films*. 2015;577: 128–133. doi:10.1016/j.tsf.2015.01.066.

[23] Kwon H, Lee SH, Kim JK. Three-dimensional metal-oxide nanohelix arrays fabricated by oblique angle deposition: fabrication, properties, and applications. *Nanoscale Res Lett*. 2015;10(369): 1–12. doi:10.1186/s11671-015-1057-2.

[24] Hawkeye MM, Joseph R, Sit JC, Brett MJ. Coupled defects in one-dimensional photonic crystal films fabricated with glancing angle deposition. *Opt Express*. 2010;18: 13220–13226. doi:10.1364/OE.18.013220.

[25] Samadi M, Zirak M, Naseri A, Khorashadizade E, Moshfegh AZ. Recent progress on doped ZnO nanostructures for visible-light photocatalysis. *Thin Solid Films*. 2016;605: 2–19. doi:10.1016/j.tsf.2015.12.064.

[26] Tseng CC, Hsieh JH, Wu W. Microstructural analysis and optoelectrical properties of Cu_2O, Cu_2O–Ag, and Cu_2O/Ag_2O multilayered nanocomposite thin films. *Thin Solid Films*. 2011;519: 5169–5173. doi:10.1016/j.tsf.2011.01.081.

[27] Taufik A, Saleha R. The influence of graphene on silver oxide synthesis through microwave assisted method. *AIP Conf Proc*. 2018;2023: 020018. doi:10.1063/1.5064015.

[28] Akkari FC, Abdelkader D, Gallas B, Kanzari M. Ellipsometric characterization and optical anisotropy of nanostructured $CuIn_3S_5$ and $CuIn_5S_8$ thin films. *Mater Sci Semicond Proc*. 2017;71: 156–160. doi:10.1016/j.mssp.2017.07.023.

[29] Tounsi N, Barhoumi A, Akkari FC, Kanzari M, Guermazi H, Guermazi S. Structural and optical characterization of copper oxide composite thin films elaborated by GLAD technique. *Vacuum*. 2015;121: 9–17. doi:10.1016/j.vacuum.2015.07.011

[30] Warren BE. *X-ray diffraction*. New York: Dover;1990.

[31] Karen P, Woodward PM. Liquid-mix disorder in crystalline solids: $ScMnO_3$. *J Solid State Chem*. 1998;141: 78–88. doi:10.1006/jssc.1998.7918.

[32] Kose S, Atay F, Bilgin V, Akyuz I. Some physical properties of copper oxide films: the effect of substrate temperature. *Mater Chem Phys*. 2008;111: 351–358. doi:10.1016/j.matchemphys.2008.04.025.

[33] Harizi A, Sinaoui A, Chaffar Akkari F, Kanzari M. Impedance spectroscopy characterization of anisotropic nano-sculptured copper oxide Cu_2O thin films for optoelectronic applications. *Mater Sci Semicond Proc*. 2016;41: 450–456. doi:10.1088/1361-6641/ab0ecf.

[34] Ehsani MH, Dizaji HR, Azizi S, Mirmahalle SFG, Siyanaki FH. Optical and structural properties of cadmium telluride films grown by glancing angle deposition. *Phys Scr*. 2013;88: 025602. doi:10.1088/0031-8949/88/02/025602.

[35] Jo H, Yang JH, Lee JH, Lim JW, Lee J, Shin M, et al. Transparent bifacial a-Si:H solar cells employing silver oxide embedded transparent rear electrodes for improved transparency. *J Sol Energy*. 2018;170: 940–946. doi:10.1016/j.solener.2018.05.096.

[36] Fakhri MA. Annealing effects on opto-electronic properties of Ag_2O films growth using thermal evaporation techniques. *Int J Nanoelectron Mater*. 2016;9: 93–102.

[37] Belgacem S, Bennaceur R. Propriétés optiques des couches minces de SnO2 et CuInS2 airless spray. *Revue Phys Appl*. 1990;25: 1245–58. doi:10.1051/rphysap:0199000250120124500.

[38] Swanepoel R. Determination of surface roughness and optical constants of inhomogeneous amorphous silicon films. *J Phys E: Sci Instrum*. 1984;17: 896.

[39] Wang S, Fu X, Xia G, Wang J, Shao J, Fan Z. Structure and optical properties of ZnS thin films grown by glancing angle deposition. *Appl Surf Sci*. 2006;252: 8734–8737. doi:10.1016/j.apsusc.2005.12.035.

[40] Woo SH, Hwangbo CK. Optical anisotropy of microstructure-controlled TiO_2 films fabricated by glancing-angle deposition (GLAD). *J Korean Phys Soc*. 2006;48: 1199–1204.

[41] Sobahan KMA, Park YJ, Hwangbo CK. Influence of deposition angle on the properties of ZrO2 thin films fabricated by using oblique angle deposition. *J Korean Phys Soc*. 2010;56: 1282–1286. doi:10.3938/jkps.56.1282.

[42] Charles C, Martin N, Devel M, Ollitrault J, Billard A. Correlation between structural and optical properties of WO_3 thin films sputter deposited by glancing angle deposition. *Thin Solid Films*. 2013;534: 275.

[43] Tauc J. Optical properties and electronic structure of amorphous Ge and Si. *Mater Res Bull*. 1968;3: 37–46. doi:10.1016/0025-5408(68)90023-8.

[44] Wei J, Lei Y, Jia H, Cheng J, Hou H, Zheng Z. Controlled in situ fabrication of Ag_2O/AgO thin films by a dry chemical route at room temperature for hybrid solar cells. *Dalton Trans*. 2014;43(29): 11333–11338. Doi:10.1039/c4dt00827h43.

[45] Varkey AJ, Fort AF. Some optical properties of silver peroxide (AgO) and silver oxide (Ag_2O) films produced by chemical-bath deposition. *Sol Energy Mater Sol Cells*. 1993;29: 253–259. doi:10.1016/0927-0248(93)90040-A.

[46] Xaba T, Moloto MJ, Al-Shakban M, Malik MA, O'Brien P, Moloto N. The effect of temperature on the growth of Ag_2O nanoparticles and thin films from bis(2-hydroxy-1-naphthaldehydato)silver(I) complex by the thermal decomposition of spin–coated films. *Mater Sci Semicond Proc*. 2017;71: 109–15.

[47] Abdelkader D, Ben Rabeh M, Khemiri N, Kanzari M. Investigation on optical properties of $Sn_xSb_yS_z$ sulfosalts thin films. *Mater Sci Semicond Proc*. 2014;21: 14–19. doi:10.1016/j.mssp.2014.01.027.

Received 2022-10-17
Accepted 2023-01-31